

1 **Maximizing Ozone Signals Among Chemical, Meteorological, and Climatological**
2 **Variability**

3
4 Benjamin Brown-Steiner^{1,2,3}, Noelle E. Selin^{2,4,5}, Ronald G. Prinn^{1,2,5}, Erwan Monier^{1,2}, Simone
5 Tilmes⁶, Louisa Emmons⁶, Fernando Garcia-Menendez⁷

6
7 *Correspondence to: Benjamin Brown-Steiner* (bbrownst@aer.com)

8 1. Center for Global Change Science, Massachusetts Institute of Technology, 77 Massachusetts Ave,
9 Cambridge, MA 02139

10 2. Joint Program on the Science and Policy of Global Change, Massachusetts Institute of Technology, 77
11 Massachusetts Ave, Cambridge, MA 02139

12 3. Now at Atmospheric and Environmental Research, 131 Hartwell Avenue, Lexington, Massachusetts, 02421

13 4. Institute for Data, Systems, and Society, Massachusetts Institute of Technology, 77 Massachusetts Ave,
14 Cambridge, MA 02139

15 5. Department of Earth, Atmospheric, and Planetary Sciences, Massachusetts Institute of Technology, 77
16 Massachusetts Ave, Cambridge, MA 02139

17 6. Atmospheric Chemistry Observations and Modeling Lab, National Center for Atmospheric Research, 3450
18 Mitchell Lane, Boulder, CO 80301

19 7. Department of Civil, Construction, and Environmental Engineering, North Carolina State University,
20 Raleigh, NC 27695

21

22 **Abstract**

23

24 The detection of meteorological, chemical, or other signals in modeled or observed air quality
25 data – such as an estimate of a temporal trend in surface ozone data, or an estimate of the mean
26 ozone of a particular region during a particular season – is a critical component of modern
27 atmospheric chemistry. However, the magnitude of a surface air quality signal is generally small
28 compared to the magnitude of the underlying chemical, meteorological, and climatological
29 variabilities (and their interactions) that exist both in space and in time, and which include
30 variability in emissions and surface processes. This can present difficulties for both policy-
31 makers and researchers as they attempt to identify the influence or 'signal' of climate trends (e.g.
32 any pauses in warming trends), the impact of enacted emission reductions policies (e.g. United
33 States NO_x State Implementation Plans), or an estimate of the mean state of highly variable data
34 (e.g. summertime ozone over the Northeastern United States). Here we examine the scale-
35 dependence of the variability of simulated and observed surface ozone data within the United
36 States and the likelihood that a particular choice of temporal or spatial averaging scales produce
37 a misleading estimate of a particular ozone signal. Our main objective is to develop strategies
38 that reduce the likelihood of overconfidence in simulated ozone estimates. We find that while
39 increasing the extent of both temporal and spatial averaging can enhance signal detection
40 capabilities by reducing the 'noise' from variability, a strategic combination of particular
41 temporal and spatial averaging scales can maximize signal detection capabilities over much of
42 the Continental US. For signals that are large compared to the meteorological variability (e.g.
43 strong emissions reductions), shorter averaging periods and smaller spatial averaging regions
44 may be sufficient, but for many signals that are smaller than or comparable in magnitude to the
45 underlying meteorological variability, we recommend temporal averaging of 10 – 15 years
46 combine with some level of spatial averaging (up to several hundred kilometers). If this level of
47 averaging is not practical (e.g. the signal being examined is at a local scale), we recommend
48 some exploration of the spatial and temporal variability to provide context and confidence in the
49 robustness of the result. These results are consistent between simulated and observed data, and
50 within a single model with different sets of parameters. The strategies selected in this study are
51 not limited to surface ozone data and could potentially maximize signal detection capabilities
52 within a broad array of climate and chemical observations or model output.

53

54 **Copyright Statement**

- 55 • Authors retain the copyright of the article. Regarding copyright transfers please see
56 below.
- 57 • Authors grant Copernicus Publications an irrevocable non-exclusive license to publish
58 the article electronically and in print format and to identify itself as the original publisher.
- 59 • Authors grant Copernicus Publications commercial rights to produce hardcopy volumes
60 of the journal for sale to libraries and individuals.
- 61 • Authors grant any third party the right to use the article freely as long as its original
62 authors and citation details are identified.
- 63 • The article is distributed under the Creative Commons Attribution 4.0 License. Unless
64 otherwise stated, associated published material is distributed under the same license.
65

66 **1 Introduction**

67 The capability to detect air quality signals – be they meteorological, chemical, or of some
68 other type – is a fundamental component of modern climate science and atmospheric chemistry.
69 The debate over the existence or length of a global warming hiatus (Lewandowski et al., 2015;
70 Roberts et al., 2015; Medhaug et al., 2017) and research examining the time of emergence of
71 climatological (Weatherhead et al., 2002; Deser et al., 2012; Hawkins and Sutton, 2012; Elía et
72 al., 2013; Schurer et al., 2013), meteorological (Giorgi and Bi, 2009; King et al., 2015), chemical
73 (Camalier et al., 2007; Strode and Pawson, 2013; Barnes et al., 2016; Garcia-Menendez et al.,
74 2017), and other sectoral signals (e.g. Monier et al., 2016) embody an accumulation of
75 techniques and strategies for filtering noise (due to natural variability) and maximizing the
76 capability to detect statistically significant signals and trends in noisy data. It is well established
77 that temporal averaging (e.g. Lewandowski et al., 2015) and spatial averaging (e.g. Frost et al.,
78 2006; Hawkins and Sutton, 2012; Barnes et al., 2016) can enhance signal detection capabilities
79 in atmospheric data. Here we extend this research by quantifying the impact of both spatial and
80 temporal averaging – individually and in combination – of surface ozone on the magnitude of the
81 calculated variability, which is largely driven by the influence of meteorological variability on
82 atmospheric chemistry (e.g. Jacob and Winner, 2009). We offer recommendations for
83 strategically averaging in space and time to maximize signal detection capabilities. In particular,
84 we examine estimates of mean ozone and of the ozone variability that results from meteorology,
85 although our approach can be generalized to other air quality applications.

86 For observed ozone data, strategies for reducing spatial and temporal noise are limited: a
87 longer time series is needed, more observations need to be made, or the spatial region over which
88 the ozone observations are being averaged needs to be enlarged. For surface ozone estimates
89 using models, however, there exist a variety of strategies for reducing the noise (due to chemical
90 and meteorological variability) relative to the strength of the signal, although they cluster into
91 three main types. The first strategy is to average or combine multiple runs of structurally
92 different models under the assumption that errors, biases, and uncertainties within the individual
93 models are reduced and the multi-model or multi-dataset mean is a best estimate of the actual,
94 aggregated ozone field. This is most notably done with multi-model ensembles within the
95 Atmospheric Chemistry and Climate Model Intercomparison Project (ACCMIP) framework
96 (Lamarque et al., 2013; Young et al., 2013; Stevenson et al., 2013), and this approach tends to

97 assume that all members in the ensemble are independent and equally skillful. This assumption,
98 however, may result in a loss of some valuable information (Knutti, 2010). Another form of this
99 strategy is to run multiple model runs within a single model, but under different initial conditions
100 or sets of parametric assumptions (e.g. Deser et al, 2012; Monier et al., 2013, 2015; Kay et al.,
101 2015; Garcia-Menendez et al., 2015, 2017). This approach cannot address structural uncertainties
102 and internal (unforced) variability between models, but is capable of identifying parametric
103 uncertainties within a single model.

104 The second strategy to reduce ozone variability is to expand the temporal averaging window,
105 which can influence the interpretation of the determined ozone value (e.g. Brown-Steiner et al.,
106 2015). The Environmental Protection Agency (EPA) National Ambient Air Quality Standard
107 (NAAQS) for ozone (US EPA, 2015) explicitly takes this into account, both in the length of the
108 averaging period (daily maximum 8-hour average) and the selection criteria for the standard
109 (fourth-highest over the previous 3 years). The calculated ozone variability can be further
110 reduced by utilizing even longer averaging periods, such as monthly (e.g. Rasmussen et al.,
111 2012), seasonal (e.g. Fiore et al., 2014; Barnes et al., 2016), annual, or decadal mean values (e.g.
112 Garcia-Menendez et al., 2017). This strategy is analogous to the averaging of meteorological
113 data to derive a climate signal, and just as Lewandowsky et al. (2015) recommend averaging 17
114 or more years in order to achieve climatological estimates of temperature trends, there is a
115 growing body of literature recommending averaging short time scale chemical variability (what
116 could be called chemical weather, see Lawrence, 2005) for 15 or more years (e.g. Garcia-
117 Menendez et al, 2017) in order to achieve an estimate of the what could be called the chemical
118 climate (see Möller, 2010).

119 The third strategy to reduce ozone variability is to average surface ozone values over larger
120 spatial regions, and while there is a significant body of literature discussing the capability and
121 interpretation of coarse resolution model representations of the sub-grid scale heterogeneity
122 (Pyle and Zavody, 1990; Searle et al., 1998, Wild et al., 2006), there are few that strategically
123 expand the spatial scale over which averaging is applied in order to maximize signal detection
124 capabilities. This strategy has been applied in other fields of the atmospheric sciences as well as
125 for general gridded datasets (e.g. Pogson and Smith, 2015), and spatial averaging has been
126 suggested as a means of reducing temperature variability and smoothing biases at the smallest
127 spatial scales within a single model run (Räisänen and Ylhäsi, 2011). This “scale problem” has

128 also been noted as an important consideration when analyzing aerosol indirect effects
129 (McComiskey and Feingold, 2012) and for the detection and attribution of extreme weather
130 events (Angélil et al., 2017).

131 Our objective in this study is to provide a framework for selecting spatial and temporal
132 averaging scales that reduces the uncertainty in analyzing ozone signals and limits the likelihood
133 of over-confidence in an estimate of surface ozone that arises from meteorological variability.
134 This type of framework can be useful from two different research perspectives. The first research
135 perspective has a priori an ozone estimate (either observed or modeled) at a certain spatial and
136 temporal scale (e.g. a 3-year simulation of surface ozone over the Northeastern US) and wants to
137 quantify the likelihood that this estimate is representative of the long-term ozone behavior (rather
138 than overly sensitive to meteorological variability of that particular 3-year period). Since ozone
139 is strongly influenced by natural fluctuations in meteorology (Jacob and Winner, 2009; Jhun et
140 al., 2015) and since extremes in surface ozone and temperature tend to co-occur (Schnell and
141 Prather, 2017), atypically hot or cold periods can strongly influence ozone behavior over short
142 time scales.

143 The second research perspective is to identify an ozone signal of a certain magnitude (or
144 threshold) and decide what spatial and temporal averaging scales are needed to best identify that
145 signal. The ozone signal could be large (e.g. determining the effectiveness or compliance with a
146 5 ppbv incremental reduction of the EPA NAAQS for ozone (US EPA, 2015)) or small (e.g.
147 identifying annual ozone trends within the US, which Cooper et al. (2012) show can be on the
148 order of 0.10 – 0.45 ppbv), and can be highly sensitivity to spatial and temporal heterogeneity
149 and meteorological variability. Barnes et al. (2016) found that surface ozone trends over 20-year
150 periods can vary by ± 2 ppbv due solely to climate variability, while interannual variability can
151 be on the order of ± 15 ppbv (Fiore et al., 2003; Tilmes et al., 2012; Lin et al., 2014) and day-to-
152 day variability can be even larger, extending regularly from near-background levels of 40 – 50
153 ppbv up to 100 ppbv during the summertime (Fiore et al., 2014).

154 In this study, we quantify the impact of both temporal and spatial averaging on the calculated
155 ozone variability – due solely to meteorological variability – in order to maximize the capability
156 to detect signals. We use simulated ozone (with the Community Atmosphere Model with
157 Chemistry, CAM-chem) and observational data (with the EPA’s Clean Air Status and Trends
158 Network, CASTNET) within the United States in order to answer the following four questions:

159 (1) Within a given dataset (model or observations), with both spatial and temporal coverage,
160 what is the magnitude of the ozone variability due to meteorology at the smallest scale, and how
161 does spatial and temporal averaging reduce this variability? (2) Are there combinations of
162 temporal and spatial averaging scales that maximize the signal detection capability for surface
163 ozone data? (3) How sensitive are the above strategies to different configurations (i.e. emissions,
164 meteorology, and climate) of the CAM-chem modeling framework? And (4) How could they be
165 applied to other datasets (chemical, meteorological, or climatological)? We limit our focus to
166 spatial scales within the United States as it has high spatial and temporal variability and
167 numerous observations, and since averaging over larger regions (e.g. the Northern Hemisphere,
168 or the globe) would produce a smaller calculated variability.

169 In Section 2, we describe the CAM-chem model and our simulations, as well as the
170 CASTNET observational database and the regional definitions used throughout this paper. In
171 Section 3 we quantify the temporal and spatial variability of surface ozone, show how temporal
172 and spatial averaging reduces the calculated ozone variability, and demonstrate the spatial
173 heterogeneity of the calculated ozone variability. In Section 4, we discuss the potential strategies
174 that could be used to maximize ozone signal detection due to meteorological variability, explore
175 uncertainties, and make recommendations for future research.

176

177 **2 Methods**

178

179 We examine both present-day (one simulation and one observed dataset) and future (two
180 simulations) surface ozone in this study. For present-day analysis, we simulate surface ozone
181 using CAM-chem, a component of the Community Earth System Model (CESM) and available
182 observations within the US from the EPA CASTNET database. For future analysis, and in order
183 to examine the potential for patterns of variability to change in the future, we utilize two existing
184 simulations of CAM-chem conducted by Garcia-Menendez et al. (2017). Much of this analysis is
185 conducted using the R language (R-Project, www.r-project.org). Here we summarize each of the
186 three datasets and our approach to our analysis in Section 3.

187

188 **2.1 CAM-chem**

189 The present-day simulation (MOZ_2000) was conducted using CAM-chem model
190 version 1.2.2, with the CAM4 atmospheric component (see Tilmes et al., 2015; 2016 for model

191 description and evaluation). The model has been used extensively for a wide range of
192 atmospheric chemistry research and is included in the ACCMIP (Lamarque et al., 2012; Young
193 et al., 2012 and references therein). We conduct our simulations using the Model for Ozone and
194 Related chemical Tracers, version 4 (MOZART-4) chemical mechanism (Emmons et al., 2010),
195 which is a full tropospheric chemical mechanism integrated into CAM-Chem (e.g. Lamarque et
196 al., 2012; Tilmes et al., 2015; Brown-Steiner et al., in review). Offline forced meteorology is
197 taken from the Modern-Era Retrospective analysis for Research and Applications (MERRA)
198 reanalysis product (Rienecker et al., 2011) for 26 meteorological years (1990 – 2015). Additional
199 model evaluation and comparisons to surface and ozonesonde observations can be found in
200 Brown-Steiner et al. (in review). This simulation has 56 vertical levels – adopted from MERRA
201 meteorology – and 96 latitudinal and 144 longitudinal grid cells. We aim to isolate the variability
202 to the meteorologically-driven impact on atmospheric chemistry so we repeat year-2000
203 anthropogenic emissions from the ACCMIP (Atmospheric Chemistry and Climate Model
204 Intercomparison Project) inventory (Lamarque et al., 2012) and all non-biogenic emissions for
205 all meteorological years, and include specified long-lived stratospheric species (O_3 , NO_x , HNO_3 ,
206 N_2O , N_2O_5) as in MOZART-4 (Emmons et al., 2010), an online biogenic emissions model
207 MEGAN (Guenther et al., 2012), and forced sea ice and sea surface temperatures to year 2000
208 historical conditions. Like many state-of-the-art chemical tracer models, the CAM-chem exhibits
209 some biases, most notably for our purposes a high bias in simulated surface ozone in the Eastern
210 US (e.g. Lamarque et al., 2012; Brown-Steiner et al., 2015; Travis et al., 2016; Barnes et al.,
211 2016). Recent efforts have been successful in partially reducing these biases (e.g. Sun et al.,
212 2017).

213 We also include two reference simulations of the future climate, MOZ_2050 and
214 MOZ_2100 (simulating the meteorological years 2035 – 2065 and 2085 – 2115, respectively)
215 using the CESM CAM-chem simulations described in detail by Garcia-Menendez et al. (2017)
216 with one set of initial condition data, and a climate sensitivity of 3.0 °C. These simulations do
217 not include projections of any changes in future emissions. Compared to the present-day
218 simulation (MOZ_2000), these future simulations (MOZ_2050 and MOZ_2100) have several
219 parametric differences: the model version is 1.1.2 (see Tilmes et al., 2015 and references for
220 information on model development), the atmospheric component is CAM3, the emissions (which
221 are held constant at year-2000 levels) are from the Precursors of Ozone and their Effects in the

222 Troposphere database (see Garcia-Menendez et al., 2017), and the meteorology is derived from a
223 linkage between the Massachusetts Institute of Technology Integrated Global System Model
224 (MIT IGSM) and the CESM CAM model (Monier et al., 2013), and as such has 26 vertical
225 levels. For a full description of these simulations, see Garcia-Menendez et al. (2017).

226

227 **2.2 CASTNET**

228 The observational database comes from the EPA Clean Air Status and Trends Network
229 (CASTNET), which has more than 90 surface observational sites within the United States and
230 has been collecting hourly surface meteorological and chemical data since 1990 (US EPA, 2016
231 and <https://www.epa.gov/castnet>). We collected data from all sites that reported complete ozone
232 data from each year and removed data that was marked invalid within the downloaded EPA files.
233 The number of sites that matched these criteria varied from year to year, but generally we have
234 between 55 and 94 sites throughout the 1991 – 2014 period. The CASTNET observational
235 network is located primarily in rural sites, and thus is considered to be a reasonable comparison
236 to coarse grid cell model output (e.g. Brown-Steiner et al., 2015; Phalitnonkiat et al., 2016).
237 Since a notable trend in observed ozone data exists, especially in the Northeastern US (Frost et
238 al., 2006), and since the simulations have no change in anthropogenic emissions, and thus no
239 ozone trend, we detrended the CASTNET data for each of the four averaging regions (described
240 below) using a simple linear regression.

241

242 **2.3 Telescoping Regional Definitions**

243 In order to isolate the impact of the size of the spatial scale over which ozone data is
244 averaged, we analyze ozone data at different spatial scales. The largest region considered is the
245 entire Continental US, while the smallest regions considered are at the individual grid cell level
246 of the CESM CAM-chem model (1.9°x2.5° latitude/longitude). Data and statistics for the other
247 regions (i.e. the Midwestern and Southeastern US) are included in the Supplemental Material,
248 but do not alter the conclusions we draw from the Northeastern US. For CESM CAM-chem data,
249 we averaged all grid cells within each region, while for the CASTNET data we first average sites
250 within each corresponding CESM CAM-chem grid cell, and then averaged these data together.
251 These telescoping regions are shown in Figure 1.

252

253 **2.4 Temporal Averaging Windows**

254 To explore the impact of temporal averaging, we examine ozone across a range of
255 temporal averaging windows, from 1 day up to the full 26 years for the CESM data (1990-2015),
256 the full 24 years for the detrended CASTNET data (1991 – 2014), and the 30 years available
257 from the future scenarios of Garcia-Menendez et al. (2017). Each averaging window, therefore,
258 can be considered to be a “sample” of possible realizations of meteorology. For instance, a
259 selection of an averaging window of 1 year has 26 possible slices within the 1990 – 2015
260 MOZ_2000 data, while a selection of an averaging window of 10 years has 17 possible slices
261 within the CESM data ($N = \# \text{ years} - \text{length of window} + 1$). In this study, we consider all
262 realizations to be equally likely and compare them to each other and to the long-term trend.
263 However, if we were only able to simulate 5 years, we would not be able to compare to the long-
264 term trend, and so be unable to completely quantify the likelihood of error in the context of the
265 long-term behavior.

266

267 **3 Results**

268 Here we examine the spatial and temporal behavior of MOZ_2000, MOZ_2050, and
269 MOZ_2100 and compare MOZ_2000 to present-day CASTNET observations. We introduce the
270 moving temporal averaging windows, explore possible thresholds of acceptable error or signal
271 strength, and examine the influence of expanding spatial averaging regions. Finally, we combine
272 these temporal and spatial averaging techniques into a single framework.

273

274 **3.1 Spatial and Temporal Comparisons**

275 Figure 2 compares summertime (JJA) maximum daily 8-hour average ozone (MDA8 O₃)
276 from the present-day model simulation (MOZ_2000, Figure 2a) to the year-2000 CASTNET
277 observations (Figure 2b). Figures 2c and 2d plot the MDA8 O₃ standard deviation and variability
278 for MOZ_2000, while Figures 2d and 2e compare the mean summertime MDA8 O₃ for the
279 future simulations (MOZ_2050 and MOZ_2100). Some of the averaging strategies we present
280 can average away the high ozone behavior this MDA8 O₃ metric is intended to quantify, but it is
281 such a well-reported metric that focusing our analysis on it allows for ready comparisons to other
282 studies. The well-known high ozone bias in the Eastern US (e.g. Lamarque et al., 2012; Travis et
283 al., 2016; Barnes et al., 2016) is apparent, but otherwise the spatial variability over the entire

284 Continental US is well captured. While we do examine the magnitude of surface ozone in this
285 paper, most of our analysis is focused on the variability around the mean value (the anomaly),
286 and as we show below, the CASTNET observations and CESM results are largely consistent in
287 their representation of ozone variability (Figure 2, Table 1). The standard deviation of the
288 simulated MDA8 O₃ is large over the Eastern US and the Pacific Coast, with peak values of ± 25
289 ppbv over the highly populated Atlantic Coast (Figure 2c). The variability (defined as the
290 standard deviation divided by the mean, expressed as a percentage) is lowest over the Western
291 US ($\sim 15\%$), only slightly higher over the Eastern US (up to 25%), and highest (up to 50%) over
292 the coastal regions (Figure 2d). We consider both the standard deviation (ppb) and a mean-
293 normalized standard deviation (as a percentage). The normalized standard deviation allows for a
294 more direct comparison of the shape of the MDA8 O₃ distributions between the simulations and
295 available observations, which accounts for the noted ozone biases (Figures 2b,c and Table 1).
296 The future climate simulations, MOZ_2050 and MOZ_2100 (Figure 2e and 2f, respectively),
297 although run with different parametric settings than MOZ_2000 (see Section 2), simulate a
298 similar spatial distribution of surface ozone, although under the warmer simulated climate of
299 2050 and 2100. These future climate simulations have a similar spatial pattern to the present-day
300 simulation (Figure 2a), with high ozone levels in the Eastern US that increases from 2050 to
301 2100 (see Garcia-Menendez et al. (2017) for more details).

302 Figure 3 compares boxplots over the four telescoping regions (Figure 1) for MOZ_2000,
303 the CASTNET data, the detrended CASTNET data, and for the single year 2000 for the
304 CASTNET data (Figures 3a-d), and Table 1 summarizes relevant statistics. In order to compare
305 CASTNET ozone to the simulated ozone, which do not have a trend over time, we detrend the
306 CASTNET data in order to remove the impact of any temporal trends (e.g. NO_x emissions
307 reductions) on ozone. The Northeastern US ozone bias is apparent at the smaller spatial scales
308 (Figures 3c,d) and is less apparent when averaging over larger regions (Figures 3a,b). Figure 3e
309 compares the year-to-year boxplots of the JJA MDA8 O₃ for the MOZ_2000 and the detrended
310 CASTNET data, and demonstrates the variability both in the median and spread of the ozone
311 values in both the modeled and simulated data. While the MOZ_2000 ozone is generally higher
312 than the CASTNET data, there are years in which the CASTNET data has higher ozone
313 extremes. The red box plot in Figure 3e, which corresponds to the red box plot in Figure 3b,

314 indicates that the year 2000 was an anomalously low year for observed ozone, although not the
315 lowest.

316 While all the CESM CAM-chem simulations have high ozone biases in the Northeastern
317 US (Figures 2 and 3, Table 1), their capability to simulate ozone variability is consistent with the
318 available observations (for present day) and for expectations of ozone variability changes in the
319 future climate (for MOZ_2050 and MOZ_2100). It is clear that variability increases when the
320 size of the averaging region decreases, a fact that is well noted in the literature, as in Hawkins
321 and Sutton (2012) for climate variables and Barnes et al. (2016) for ozone. As can be seen in in
322 Table 1, the CASTNET variability increases as the spatial scale decreases (10%, 13%, 16%, and
323 20% for our telescoping regions from continental to a single Northeastern U.S. grid box), and
324 MOZ_2000 largely captures this trend, albeit with lower overall variability (5%, 10%, 15%, and
325 15%). This increase in ozone variability with decreasing spatial scale is maintained in the future
326 climate simulations (6%, 10%, 16%, and 21% for MOZ_2050 and 7%, 12%, 17%, and 20% for
327 MOZ_2100). Table S1 contains statistics for the other telescoping regions.

328
329

330 **3.2 Variability, Averaging Windows, and Thresholds**

331 As we aim to quantify the potential tradeoffs that result from a particular choice of
332 temporal and spatial scales on the assessment of ozone variability within the US, we represent
333 the spatial scale by applying the telescoping regions (see Figure 1 and Section 2.3) and we
334 represent the temporal scale through the use of moving averaging windows (see Section 2.4). We
335 frame much of the following analysis from the perspective of limited simulation length in order
336 to approximate the question that decision-makers and modelers face when constrained by limited
337 computational capabilities or available data: what is the likelihood that a particular estimate (of
338 both the mean and the variability) is not a true representation of the true mean and variability, but
339 rather a product of the underlying variability at the particular choice of spatial and temporal
340 scale?

341 Figure 4 presents this likelihood by plotting all possible estimates of MDA8 O₃ (as
342 anomalies from the long-term mean) over all possible selections of averaging window (from 1
343 day up to the complete time series) for our telescoping regions. The semi-cyclical and highly
344 auto-correlated nature of surface ozone is apparent at all spatial scales, with alternating cycles of
345 anomalously high and low ozone. The temporal impact of anomalous ozone events is indicated

346 by the vertical and right-leaning diagonal striations, which show that anomalous ozone events
347 can impact estimates of ozone values within averaging windows up to 15 or 20 years. Figure 4
348 demonstrates how small-scale anomalously high or low ozone values (that come only from
349 meteorological variability) can impact temporal averages of 5, 10, or even 20 years. For instance,
350 a selected 5-year averaging window within the MOZ_2000 simulation averaged over the
351 Northeastern US could be 2.5 ppbv higher or lower than the 25-year mean value of 74 ppbv, a
352 potential error of 7%. Horizontal lines in Figure 4 mark the length of averaging windows that are
353 needed to ensure that ozone anomaly for any selection of averaging window does not exceed a
354 given threshold (5, 1, and 0.5 ppbv for solid, dashed, and dotted lines respectively). This
355 potential error is larger within smaller regions and at the shorter selections of the averaging
356 window. While the high and low ozone anomalies differ in time between CASTNET,
357 MOZ_2000, MOZ_2050, and MOZ_2100 in Figure 4, the impact of spatial and temporal
358 averaging is consistent.

359 We also quantify this variability in Supplemental Figures S1 and S2, which plots the
360 likelihood (as a percentage) that a particular selection of spatial (rows) and temporal (x-axis)
361 scale estimates ozone values that exceed a particular threshold (colored lines) away from the true
362 mean value. For instance, if we are interested in characterizing ozone behavior (e.g. estimating a
363 trend, or the mean value) in the Northeastern US, but were limited to a 5-year simulation, there is
364 more than a 50% likelihood that the simulated ozone is 1 ppbv away from the 26-year mean, and
365 an 80% likelihood that the discrepancy is greater than 0.5 ppbv. However, these data indicate
366 that there is a virtual certainty that the estimate will be within 2.5 ppbv of the true mean value.
367 We should note that, at the grid-cell level and within a 10-year period, the surface ozone
368 variability can exceed 1 ppbv but is unlikely to exceed 2.5 ppbv (Figure 4), and that a 20-year
369 trend is very likely to be able to identify significant ozone signals among the impact of
370 meteorological variability on atmospheric chemistry. Our results also align with the results from
371 Garcia-Menendez et al. (2017), which recommended that simulations need to be at least 15 years
372 long to identify anthropogenically-forced ozone signals on the order of 1 ppbv.

373 Figures 4 and Supplemental Figures S1 and S2 compare the CASTNET observations to
374 the three CESM CAM-chem simulations, and while there are minor differences, there are broad
375 features that are consistent. First, using longer temporal averaging windows reduces the
376 influence of small-scale ozone variability at all spatial scales, and depending on the acceptable

377 threshold, one can select a temporal scale that effectively reduces the likelihood of exceeding
378 that threshold to zero. Second, larger spatial scales also reduce this likelihood of exceeding a
379 given threshold, but not as effectively as longer temporal scales. Finally, the impact of both
380 temporal and spatial averaging on ozone variability is largely consistent for the CASTNET
381 observations and for all three CESM CAM-chem simulations.

382

383 **3.3 Selection of Temporal Averaging Scales**

384 Figure 5 extends this analysis to examine the spatial heterogeneity of this likelihood of
385 the meteorological variability causing ozone anomalies exceeding particular thresholds at the
386 grid cell level. Here we plot four thresholds (0.5, 1, 2.5, and 5 ppbv) and four averaging windows
387 (1, 5, 10, and 20 years) for the MOZ_2000 simulation. Ozone variability is highest in the Eastern
388 US. At the grid-cell level, there are two strategies for filtering out the noise associated with
389 natural meteorological variability (and thus enhancing signal detection capabilities): either
390 average over longer periods, or acknowledge the level of noise and increase the threshold. For
391 these data, it is virtually certain that any 20-year average will be within 5 ppbv of a full 25-year
392 mean value (which itself may not be an accurate representation of a longer simulation), and
393 virtually certain that any 1-year average will be at least 0.5 ppbv away from the mean.

394 Supplemental Figure S3 extends the analysis of Figure 5 by comparing the MOZ_2000,
395 MOZ_2050, and MOZ_2100 simulations across the four thresholds for the 5-year averaging
396 window. Figure 6 similarly compares the 1 ppbv ozone threshold across the four averaging
397 windows for MOZ_2000, MOZ_2050, and MOZ_2100. Interpreting Figures 6 and Supplemental
398 Figure S3 give largely consistent interpretations than the analysis above (Figure 5). Namely, that
399 at the grid-scale level, increasing the temporal averaging window (Figure 6) or increasing the
400 acceptable ozone threshold (Supplemental Figure S3) are effective at reducing the impact of the
401 meteorological variability on estimates of the ozone signal. Shorter windows (or smaller
402 thresholds) are needed in the Western US (where variability is smaller, see Figure 2d) than in the
403 Eastern US (where variability is larger) as well as over coastal and highly populated regions.
404 Finally, the 1 ppbv threshold and the 5-year averaging window plots (in either Figure 5 or
405 Supplemental Figure S3) indicate that the spatial distribution and location of the peak variability
406 may shift into the future, although this may be due to parametric differences between

407 MOZ_2000, MOZ_2050, and MOZ_2100. Future simulations will be needed to check this shift
408 in peak ozone variability.

409

410 **3.4 Selection of Spatial Averaging Scales**

411 We examine the impact of increasing the spatial averaging region (Figure 7) at four
412 different temporal averaging windows (1, 5, 10, and 20 years) and for the smallest ozone
413 threshold from the previous section (0.5 ppbv). It is evident that at all temporal averaging
414 windows, expanding the number of surrounding grid cells that are averaged together consistently
415 decreases the likelihood of exceeding the 0.5 ppbv threshold, although these reductions are
416 relatively small at the 1-year window, especially over the Eastern U.S. While increasing the
417 spatial averaging from a single grid-cell up to include the surrounding 81 grid cells (bottom row
418 in Figure 7) manages to essentially smooth away much of the spatial heterogeneity in surface
419 ozone (by moving down any column in Figure 7), it does not eliminate the likelihood of
420 exceeding the 0.5 ppbv threshold over much of the Eastern U.S. For instance, even at a 20-year
421 averaging window, and by averaging together the surrounding 81 grid-cells over locations in the
422 Eastern U.S., there is still a 20-70% likelihood of exceeding the 0.5 ppbv threshold due to the
423 small-scale impact of the meteorological variability on atmospheric chemistry.

424

425 **3.5 Combination of Spatial and Averaging Scales**

426 We now examine the combined impact of temporal and spatial averaging on reducing the
427 influence of small-scale ozone variability in order to enhance ozone signal detection capabilities.
428 Table S2 summarizes our analysis by dividing the likelihood of the ozone variability estimates
429 exceeding selected thresholds away from the long-term mean into four categories: (1) the length
430 of the averaging window over which ozone is averaged (columns); (2) the magnitude of the
431 ozone threshold of interest (rows); (3) the observed (CASTNET) and modeled (MOZ_2000,
432 MOZ_2050, and MOZ_2100) ozone data (sub-columns); and (4) the size of the spatial extent
433 over which ozone is averaged (sub-rows). A graphical representation consistent with the data
434 presented in Table S2 is plotted in Figure 8 for the Continental US average and for three grid
435 cells that represent various cases. In each plot in Figure 8, by moving along columns from left to
436 right, we can see the influence of increasing the size of the temporal averaging window, and by
437 moving along rows (from the bottom to the top), we can see the influence of increasing the

438 spatial averaging scale. By taking in the entire plot as a whole, we can get a feel for the
439 combined influence of both temporal and spatial averaging. Supplemental Figure S4 contains a
440 plot for each grid cell in the Continental US.

441 On average within the Continental US, both temporal and spatial averaging are effective
442 at reducing the calculated MDA8 O₃ anomaly, although temporal averaging is more effective
443 (Figure 8a). There are many grid cells in the Eastern and Western US coasts (Figure 8b,
444 Supplemental Figure S4), where both spatial and temporal averaging are effective, but their
445 combined usage is especially effective. There are also many grid cells where temporal averaging
446 is effective, but spatial averaging is barely effective, or not effective at all (Figure 8c and
447 Supplemental Figure S4). Finally, there are some grid cells, particularly in the Central US
448 (Figure 8d and Supplemental Figure S4), where spatial averaging over smaller regions is
449 effective, but spatial averaging of larger regions actually increases the calculated MDA8 O₃
450 anomaly by including surrounding grid cells that have higher variability.

451

452 **4 Discussion**

453 We now return to the original four research questions posed in Section 1. First, what is
454 the magnitude of ozone variability due to meteorology alone at the smallest scale, and what is the
455 impact of increasing the scale of temporal and spatial averaging? In both observed and modeled
456 MDA8 O₃ surface data, the small-scale variability driven solely by the meteorological variability
457 impact on atmospheric chemistry (expressed as the standard deviation as a percentage of the
458 mean) can exceed 20% (Table 1, Figure 2d). The chemical variability examined here is the result
459 of fluctuations in meteorology, which itself results from larger-scale climatological drivers.
460 While variability in emissions also influences atmospheric chemistry, our analysis has removed
461 the influence of emissions variability and isolated the variability due to meteorology. A more
462 comprehensive analysis of chemical variability will need to account for both meteorological and
463 emission variability, which is complicated by temporal trends in both the emissions of ozone
464 precursor species and the climate.

465 There is high temporal and spatial heterogeneity of surface ozone variability (Figure 2d),
466 with the lowest values found in the Western US (< 10%), higher values found in the Eastern US
467 (up to 20%), and the highest values over coastal or heavily populated regions (up to 30%).
468 Averaging over longer temporal scales (by increasing the averaging window) and over larger

469 spatial scales (by expanding the averaging region) can reduce the magnitude of the calculated
470 variability, with temporal averaging proving to be more effective than spatial averaging in most
471 cases (Figure 8). In this study, we performed simple spatial averaging, but there are other
472 methodologies for smoothing two-dimensional signals (e.g. Räisänen et al., 2011; Pogson and
473 Smith, 2015) that could potentially increase signal detection capabilities.

474 Second, are there combinations of temporal and spatial averaging that maximize the
475 filtration of calculated ozone variability, and thus maximize the potential for signal detection?
476 Figure 8 (and Supplemental Figure S4) demonstrate clearly that there are cases in which the
477 combined usage of temporal and spatial averaging can reduce the calculated variability better
478 than either strategy alone (see Figure 8b), although there are many regions within the Eastern US
479 in which spatial averaging has little to no impact on reducing the calculated variability (Figure
480 8c) or even results in an increase in the calculated variability (Figure 8d). There are no such
481 cases (see Supplemental Figure S4) in which expanding the temporal averaging scale increases
482 the calculated ozone variability. This could potentially enable region-specific averaging
483 strategies that help decision-makers identify and meet regional air quality objectives.

484 Third, are these results dependent on the particular parameterizations of the CESM
485 CAM-chem model, and are they consistent with the available CASTNET observations? The
486 three CESM CAM-chem simulations exhibited consistent representations of ozone variability,
487 consistent with our understanding of future changes to the climate (and meteorology) and the
488 resulting impact on atmospheric chemistry (Table 1, Figures 4, S1, and S2). Compared to the
489 CASTNET observations (which we detrended to remove the influence of changing precursor
490 emissions), the present-day simulation (MOZ_2000) exhibited a high ozone bias in the Eastern
491 US, while the representation of the ozone variability is comparable (Table 1).

492 Fourth, how may these strategies be applied to other datasets, be they chemical,
493 meteorological, or climatological? Much of this analysis could be applied to any dataset that has
494 spatial and temporal coverage, as long as some set of acceptable thresholds is provided. While
495 our time step in this analysis is daily (given the MDA8 O₃ metric), and applied only to
496 summertime (JJA) days, any time step (i.e. hourly, monthly, annual, decadal) could be utilized as
497 long as cyclical trends (e.g. diurnal or seasonal cycles) are removed. Indeed, the sliding-scale
498 presentation in Figure 8 and Supplemental Figure S4 can specifically be utilized to identify
499 particular spatial and temporal scales that are sufficient to identify signals at particular thresholds

500 and to identify particular geographic regions that are best suited to identify a given signal. For
501 example, Sofen et al. (2016) identified regions across the globe where additional observations
502 would be particularly suited to improve our understanding of surface ozone behavior, and our
503 analysis could potentially be used to identify particular temporal and spatial averaging scales that
504 could further maximize the capability for trend detection. In particular, Sofen et al. (2016) noted
505 that the peak in the power spectrum of the El Niño-Southern Oscillation (ENSO) on surface
506 ozone is at the 3.8 year time scale, and that within some regions within the US, the amplitude of
507 the ENSO influence on surface ozone approached 0.5 ppbv (and up to 1.1 ppbv globally). Our
508 analysis shows that there are no grid cells within the Continental US where a 0.5 ppbv signal can
509 be identified at the 5-year (or shorter) temporal averaging scale (Supplemental Figure S4), but
510 that there are many regions – especially within the Western US – in which even a modest amount
511 of spatial averaging can identify surface ozone signals below the 1 ppbv level with a 5-year or
512 shorter averaging window. The type of sliding-scale analysis – in which spatial and temporal
513 averaging are utilized individually and in combination – as presented in Figure 8 and
514 Supplemental Figure S4 could readily be applied to a wide range of atmospheric (and other)
515 topics to aid in the capability to identify signals that exist both in space and in time. In particular,
516 low-frequency oscillations (e.g. ENSO, and others) and other forms of internally or externally
517 forced trends (e.g. anthropogenic and natural changes in emissions) are readily adaptable to this
518 type of analysis, which could address signals pertaining to precipitation, biogenic emissions,
519 boundary layer variables, cloud properties, and many others.

520 We did not quantify statistical significance (as in Lewandowski et al., 2015) as our goals
521 were to understand the general nature of ozone variability at all scales and for all signal
522 strengths. Statistical significance testing (and other statistical techniques) can certainly provide
523 additional information as to the strengths of ozone signals within the underlying variability, and
524 can be used to extend these results in a case-by-case manner, but we leave this testing to future
525 studies that can focus on particular air quality objectives at particular temporal and spatial scales.
526 Furthermore, future research examining the impact of spatial and temporal averaging using
527 regional-scale models, models with different resolutions, and the inclusion of urban observations
528 could provide additional insight into understanding chemical variability and averaging
529 techniques.

530 Smaller signals require longer temporal averaging periods to identify. Figure 4 shows that
531 a 0.5 ppb MDA8 O₃ signal will emerge after 15 - 20 years of temporal averaging. The range here
532 reflects different spatial averaging domains, with larger domains requiring shorter temporal
533 averaging windows than smaller domains (i.e. 15 years for averaging over the Continental US
534 and 20 years for averaging over the Northeastern US). This would mean that an average trend of
535 0.25 - 0.33 ppb/year would require a time series of at least 15 years to identify. Similarly, a 1.0
536 ppb MDA8 O₃ signal emerges after 7 - 15 years, which indicates an average trend of 0.14 - 0.67
537 ppb/year would take at least 7 years to identify. Finally, a 5 ppb signal can be identified in less
538 than 3 years, which indicates that an average trend of 1.67 ppb/year or greater would only require
539 a 3-year time series. This presents particular difficulties if the ozone signal of interest is a trend
540 spanning a time period on the same order. The 10 - 15 year averaging time scale we propose
541 translates into a length of time beyond which you are likely to not see spurious trends above 0.5
542 ppb, but there are many cases in which the identification of a small trend is desired with less than
543 10 - 15 years of available data. For instance, Jiang et al. (2018) have found that NO_x emissions
544 reductions since 2005 are not as strong as previously expected, showing a significant slowdown
545 beginning in 2011. This has large implications for ozone and for short-term decisions for air
546 quality managers within the United States, who have to promulgate policies on short-term scales
547 without the luxury of postponing action until longer and more complete data sets become
548 available. As we have shown, spatial and temporal variability due to meteorology is high, and the
549 identification and quantification of trends over 5, 10, or 15 years is difficult, particularly at small
550 spatial scales.

551 However, as we have shown, a consideration of the impact on variability – and how
552 variability changes over time – is often pivotal to understand the nature of the signals being
553 examined. In this paper, we have provided methods for quantifying the spatial and temporal
554 variability and strategies for determining which types of signals are likely detectable at particular
555 temporal and spatial scales. Some signals, especially small signals at small scales, are simply not
556 large enough to emerge from the variability, and thus may not be detectable without additional
557 data or expanding the temporal and spatial averaging scales used for analysis. Quantifying the
558 signal-to-noise ratio at a variety of spatial scales, and determining an acceptable threshold of a
559 particular signal, could be one accessible method for providing this context. The risk in
560 neglecting the quantification and contextualization of the magnitude of the ozone signal relative

561 to the magnitude of the variability induced by the internal meteorology – and the impact of
562 temporal and spatial averaging – is primarily the risk of drawing conclusions that are more
563 sensitive to a particular peculiarity in the underlying variability rather than the signal itself.

564

565 **5 Conclusions**

566 We quantified the impact of spatial and temporal averaging at different scales – both
567 individually and combined – on estimates of summertime surface ozone variability and the
568 resulting likelihood of over-confidence in estimates of chemical signals over the United States
569 using CASTNET observations and the CESM CAM-chem model. We simulate three multi-
570 decadal time periods, each with constant surface emissions, and find that this analysis is
571 consistent across our simulated time periods, and that our results are not sensitive to particular
572 configurations and parametric choices within the CESM CAM-chem (i.e. emissions,
573 meteorology, and climate). We also provide a conceptual framework for gaining understanding
574 of the influence of spatial and temporal averaging that may be adapted to a wide range of
575 atmospheric and surface phenomena, provided sufficient spatial and temporal coverage. Here we
576 focus on summertime surface ozone, a highly variable (in both space and time) atmospheric
577 constituent with severe human health impacts and implications for planetary climate, which is
578 the focus of many local, regional, and national policies. However, these ozone signals (e.g.
579 temporal trends or regional averages) are frequently small when compared to the magnitude of
580 the day-to-day ozone variability, and thus detecting these signals can be challenging. In
581 particular, it would be impractical to delay interpreting observations for 10 – 15 years, or
582 alternatively to expand the spatial averaging such that small-scale features are smoothed away.
583 Nonetheless, it is unwise to over-interpret trends and signals based on observations from a
584 limited spatial area and over a short temporal period. Our analysis and conceptual framework
585 presented here cannot solve this tension, but it does demonstrate some strategies which can allow
586 for a selection of spatial and temporal averaging scales, and a consideration of the error
587 threshold, that can aid in this signal detection on a case-by-case basis. Taking into account the
588 complex interactions involving trends and variability between emissions, chemistry,
589 meteorology, and climatology necessitates a variety of strategies. This work quantifies the
590 impact of spatial and temporal averaging in signal detection, which can be used in conjunction

591 with ensembles of simulations, statistical techniques, and other strategies to further our
592 understanding of the chemical variability in our atmosphere.

593 In order to quantify the impact of spatial and temporal averaging on summertime ozone
594 variability, we start by selecting four telescoping spatial regions (the Continental US, the Eastern
595 US, the Northeastern US, and a single grid cell within the Northeastern US) and examine all
596 possible choices for averaging windows (ranging from daily to multi-decadal windows),
597 although we focused primarily on averaging windows of 1, 5, 10, and 20 years. We find that –
598 consistent with previous studies – summertime MDA8 O₃ variability is largest at the smallest
599 spatial and temporal scales, and is frequently on the order of $\pm 10 - 20$ ppbv, or which is roughly
600 15-20% of the mean ozone signal. In order to minimize the chemical noise that results from
601 meteorological variability – and thus enhance the signal – we find averaging windows of 10-15
602 years (and sometimes longer at the smaller spatial scales) combined with modest (nearest-
603 neighbor) spatial averaging substantially improve the capability for signal detection. For signals
604 that are large compared to the underlying meteorological variability (e.g. strong emissions
605 reductions), shorter averaging windows and smaller spatial regions may be used. We recognize
606 that achieving a 10 – 15 year temporal averaging window is difficult, but this recommendation is
607 consistent with recent literature (e.g. Barnes et al., 2015; Garcia-Menendez et al., 2017). For
608 studies where 10 – 15 years of averaging is impractical, we recommend that some spatial and
609 temporal context is provided that demonstrates that the signals being examined are robust and
610 not the result of internal variability or noise. We also recognize that our analysis is just one
611 strategy for enhancing signal detection capabilities, and will ideally be used alongside others,
612 such as perturbed initial condition ensembles, running simulations with either internal or forced
613 meteorology, and examining a region or time period with different models or parameterizations.

614 We show that the largest summertime ozone variability is found in the Eastern US (Figure 5,
615 Figure S4), and subsequently there are many regions within the Eastern US where even a 20-year
616 averaging window has a non-negligible likelihood of estimating ozone variability that is
617 dependent (with possible error in the 1 – 3 ppbv range) on the particular years selected. In
618 addition, over much of the Eastern US, simulations of 5-years or shorter have a substantial
619 likelihood (40 – 90%, Figures S1 and S2) of reflecting the influence of meteorological variability
620 on chemistry rather than the mean state of surface ozone, with the possibility of 5 – 10 ppbv
621 error (Figure S4). While we have detrended the CASTNET observations to compare to the

622 constant year-2000 cycled emissions in the simulations, the CASTNET time series inherently
623 includes the compounded variability of both meteorological and emission sources. Future studies
624 will need to expand this analysis to include trends and variability in the emissions, as well as in
625 the meteorology.

626 Finally, we demonstrate a conceptual framework that allows for a “sliding-scale” view of
627 surface ozone variability, in which both temporal and spatial averaging is examined at every grid
628 cell within the Continental US. We show that the magnitude of estimates of ozone variability can
629 be reduced with both temporal and spatial averaging, although temporal averaging tends to be
630 more effective. While there are many regions in which both temporal and spatial averaging used
631 in conjunction substantially reduce the estimate of ozone variability, there are some regions
632 where spatial averaging is ineffective, or even counter-effective. In contrast, this is not the case
633 for temporal averaging, which consistently reduces the magnitude of estimated ozone variability.
634 Our analysis could be combined with other studies (e.g. Sofen et al., 2016) to guide
635 observational and modeling strategies and identify regions and scales at which particular signals
636 are most likely to be identified.

637

638 **Code Availability**

639 CESM CAM-Chem code is available through the National Center for Atmospheric Research /

640 University Corporation for Atmospheric Research (NCAR/UCAR) website

641 (<http://www.cesm.ucar.edu/models/cesm1.2/>), and this project made no code modifications from

642 the released model version.

643 **Data Availability**

644 The raw model output is archived on the NCAR servers, and processed data is archived at
645 <https://dspace.mit.edu/handle/1721.1/114467>.

646 **Supplemental Link**

647

648 **Author Contribution**

649 BBS ran the present-day simulation, analyzed the data, and wrote the manuscript. EM ran the
650 future climate simulations, while FGM ran the future atmospheric chemistry simulations and
651 made the data available to BBS. NS, RP, EM, ST, and LE guided and reviewed the scientific
652 modeling and analysis process. All authors provided feedback throughout the project and
653 development of the manuscript.

654

655 **Competing Interests**

656 The authors declare that they have no conflict of interest.

657

658 **Acknowledgements**

659 This model development work was supported by the U.S. Department of Energy (DOE) Grant
660 DE-FG02-94ER61937 to the MIT Joint Program on the Science and Policy of Global Change.
661 Computational resources for this project were provided by DOE and a consortium of other
662 government, industry, and foundation sponsors of the Joint Program. For a complete list of
663 sponsors, see: <http://globalchange.mit.edu>. Additional computing resources were provided by the
664 Climate Simulation Laboratory at NCAR's Computational and Information Systems Laboratory
665 (CISL), sponsored by the National Science Foundation and other agencies. The National Center
666 for Atmospheric Research is funded by the National Science Foundation. The authors would also
667 like to thank Daniel Rothenberg for efficient processing of the ozone files.

668

669 **References**

- 670 Angéilil, O., Stone, D., Perkins-Kirkpatrick, S., Alexander, L.V., Wehner, M., Shiogama, H.,
671 Wolski, P., Ciavarella, A., and Christidis, N.: On the nonlinearity of spatial scales in
672 extreme weather attribution statements, *Clim. Dyn.*, 2017.
- 673 Barnes, E. A., Fiore, A. M., and Horowitz, L. W.: Detection of trends in surface ozone in the
674 presence of climate variability, *J. Geophys. Res. Atmos.*, 121, 6112–6129, 2016.
- 675 Brown-Steiner, B., Hess, P. G., and Lin, M. Y.: On the capabilities and limitations of GCCM
676 simulations of summertime regional air quality: A diagnostic analysis of ozone and
677 temperature simulations in the US using CESM CAM-chem, *Atmos. Environ.*, 101, 134–
678 148, 2015.
- 679 Brown-Steiner, B., Selin, N. E., Prinn, R., Tilmes, S., Emmons, L., Lamarque, J.-F., and
680 Cameron-Smith, P.: Evaluating Simplified Chemical Mechanisms within CESM Version
681 1.2 CAM-chem (CAM4): MOZART-4 vs. Reduced Hydrocarbon vs. Super-Fast Chemistry,
682 *Geosci. Model Dev. Discuss.*, in review, 2018.
- 683 Camalier, L., Cox, W., and Dolwick, P.: The effects of meteorology on ozone in urban areas
684 and their use in assessing ozone trends, *Atmos. Environ.*, 41, 7127-7137, 2007.
- 685 Cooper, O. R., Gao, R. S., Tarasick, D., Leblanc, T., and Sweeney, C.: Long-term ozone trends
686 at rural ozone monitoring sites across the United States, 1990-2010, *J. Geophys. Res.*, 117,
687 D22307, 2012.
- 688 de Elía, R., Biner, S., and Frigon, A.: Interannual variability and expected regional climate
689 change over North America, *Clim. Dyn.*, 41, 1245, 2013.
- 690 Deser, C., Phillips, A., Bourdette, V., and Teng, H.: Uncertainty in climate change projections:
691 the role of internal variability, *Clim. Dyn.*, 38, 527, 2012.
- 692 Diem, J. E., and Comrie, A. C.: Predictive mapping of air pollution involving sparse spatial
693 observations, *Environmental Pollution*, 119, 1, 99–117, 2002.
- 694 Emmons, L. K., Walters, S., Hess, P. G., Lamarque, J.-F., Pfister, G. G., Fillmore, D., Granier,
695 C., Guenther, A., Kinnison, D., Laepple, T., Orlando, J., Tie, X., Tyndall, G., Wiedinmyer,
696 C., Baughcum, S. L., and Kloster, S.: Description and evaluation of the Model for Ozone
697 and Related chemical Tracers, version 4 (MOZART-4), *Geosci. Model Dev.*, 3, 43-67,
698 2010.
- 699 Fiore, A. M., Oberman, J. T., Lin, M. Y., Zhang, L., Clifton, O. E., Jacob, D. J., Naik, V.,
700 Horowitz, L. W., Pinto, J. P., and Milly, G. P.: Estimating North American background
701 ozone in U.S. surface air with two independent global models: Variability, uncertainties,
702 and recommendations, *Atmos. Environ.*, 96, 284–300, 2014.
- 703 Fiore, A. M., Jacob, D. J., Liu, H., Yantosca, R. M., Fairlie, T. D., and Li, Q.: Variability in
704 surface ozone background over the United States: Implications for air quality policy, *J.*
705 *Geophys. Res. Atmos.*, 108, D24, 1787, 2003.
- 706 Garcia-Menendez, F., Saari, R. K., Monier, E., and Selin, N. E.: U.S. Air Quality and Health
707 Benefits from Avoided Climate Change under Greenhouse Gas Mitigation, *Environ. Sci.*
708 *Technol.*, 49, 7580–7588, 2015.

709 Garcia-Menendez, F., Monier, E., and Selin, N. E.: The role of natural variability in projections
710 of climate change impacts on U.S. ozone pollution, *Geophys. Res. Lett.*, 44, 2911–2921,
711 2017.

712 Giorgi, F., and Bi, X.: Time of emergence (TOE) of GHG-forced precipitation change hot-spots,
713 *Geophys. Res. Lett.*, 36, L06709, 2009.

714 Guenther, A. B., Jiang, X., Heald, C. L., Sakulyanontvittaya, T., Duhl, T., Emmons, L. K., and
715 Wang, X.: The Model of Emissions of Gases and Aerosols from Nature version 2.1
716 (MEGAN2.1): An extended and updated framework for modeling biogenic emissions,
717 *Geosci. Model Dev.*, 5, 1471–1492, 2012.

718 Hawkins, E., and Sutton, R.: Time of emergence of climate signals, *Geophys. Res. Lett.*, 39,
719 L01702, 2012.

720 Jacob, D. J., and Winner, D. A.: Effect of climate change on air quality, *Atmos. Environ*, 43, 51–
721 63, 2009.

722 Jiang, Z., McDonald, B. C., Worden, H., Worden, J. R., Miyazaki, K., Qu, Z., Henze, D. K.,
723 Jones, D. B. A., Arellano, A. F., Fischer, E. V., Zhu, K., and Boersma, F.: (2018).
724 Unexpected slowdown of US pollutant emission reduction in the past decade. *Proceedings*
725 *of the National Academy of Sciences*, 201801191.

726 Jhun, I., Coull, B. A., Schwartz, J., Hubbell, B., and Koutrakis, P.: The impact of weather
727 changes on air quality and health in the United States in 1994–2012, *Environ. Res. Lett.*, 10,
728 084009, 2015.

729 Kay, J. E., Deser, C., Phillips, A., Mai, A., Hannay, C., Strand, G., Arblaster, J. M., Bates, S. C.,
730 Danabasoglu, G., Edwards, J., Holland, M., Kushner, P., Lamarque, J.-F., Lawrence, D.,
731 Lindsay, K., Middleton, A., Munoz, E., Neale, R., Oleson, K., Polvani, L., and Vertenstein,
732 M.: The Community Earth System Model (CESM) large ensemble project: A community
733 resource for studying climate change in the presence of internal climate variability, *Bull.*
734 *Amer. Meteor. Soc.*, 96, 1333–1349, 2015.

735 King, A. D., Donat, M. G., Fischer, E. M., Hawkins, E., Alexander, L. V, Karoly, D. J., Dittus,
736 A. J., Lweis, S. C., and Perkins, S. E.: The timing of anthropogenic emergence in simulated
737 climate extremes, *Environ. Res. Lett.*, 10, 094015, 2015.

738 Knote, C., Tuccella, P., Curci, G., Emmons, L., Orlando, J. J., Madronich, S., Baró, R., Joménez-
739 Guerrero, P., Luecken, D., Hogrefe, C., Forkel, R., Werhahn, J., Hirtl, M., Pérez, J. L., José,
740 R. S., Giordano, L., Brunner, D., Yahya, K., and Zhang, Y.: Influence of the choice of gas-
741 phase mechanism on predictions of key gaseous pollutants during the AQMEII phase-2
742 intercomparison, *Atmos. Environ.*, 115, 553–568, 2015.

743 Knutti, R.: The end of model democracy?, *Clim. Change*, 102, 395–404, 2010.

744 Lamarque, J.-F., Bond, T. C., Eyring, V., Granier, C., Heil, A., Klimont, Z., Lee, D., Liousse, C.,
745 Mieville, A., Owen, B., Schultz, M. G., Shindell, D., Smith, S. J., Stehfest, E., Van
746 Aardenne, J., Cooper, O. R., Kainuma, M., Mahowald, N., McConnell, J. R., Naik, V.,
747 Riahi, K., and Van Vuuren, D. P.: Historical (1850–2000) gridded anthropogenic and
748 biomass burning emissions of reactive gases and aerosols: Methodology and application,
749 *Atmos. Chem. Phys.*, 10, 7017–7039, 2010.

750 Lamarque, J.-F., Dentener, F., McConnell, J., Ro, C.-U., Shaw, M., Vet, R., Bergmann, D.,
751 Cameron-Smith, P., Dalsoren, S., Doherty, R., Faluvegi, G., Ghan, S. J., Josse, B.,
752 MacKenzie, I. A., Plummer, D., Shindell, D. T., Skeie, R. B., Stevenson, D. S., Strode, S.,
753 Zeng, G., Curran, M., Dahl-Jensen, D., Das, S., Fritzsche, D., and Nolan, M.: Multi-model
754 mean nitrogen and sulfur deposition from the atmospheric chemistry and climate model
755 intercomparison project (ACCMIP): Evaluation of historical and projected future changes,
756 *Atmos. Chem. Phys.*, 13, 7997–8018, 2013.

757 Lamarque, J.-F., Emmons, L. K., Hess, P. G., Kinnison, D. E., Tilmes, S., Vitt, F., Heald, C. L.,
758 Holland, E. A., Lauritzen, P. H., Neu, J., Orlando, J. J., Rasch, P. J., and Tyndall, G. K.:
759 CAM-chem: Description and evaluation of interactive atmospheric chemistry in the
760 Community Earth System Model, *Geosci. Model Dev.*, 5, 369–411, 2012.

761 Lawrence, M. G., Hov, Ø., Beekmann, M., Brandt, J., Elbern, H., Eskes, H., Feichter, H., and
762 Takigawa, M.: The chemical weather, *Environ. Chem*, 2, 6–8, 2005.

763 Lewandowsky, S., Risbey, J. S., and Oreskes, N.: On the definition and identifiability of the
764 alleged “hiatus” in global warming, *Sci. Rep.*, 5, 16784, 2015.

765 Lin, M., Horowitz, L. W., Oltmans, S. J., Fiore, A. M., and Fan, S.: Tropospheric ozone trends at
766 Mauna Loa Observatory tied to decadal climate variability, *Nat. Geosci.*, 7, 136–143, 2014.

767 McComiskey, A., and Feingold, G.: The scale problem in quantifying aerosol indirect effects,
768 *Atmos. Chem. Phys.*, 12, 1031–1049, 2012.

769 Medhaug, I., Stolpe, M. B., Fischer, E. M., and Knutti, R.: Reconciling controversies about the
770 ‘global warming hiatus,’ *Nature*, 545, 41–47, 2017.

771 Möller, D. *Chemistry of the Climate System*, pp. 331-334, Walter de Gruyter GmbH and Co.,
772 KG, Berlin/New York, 2010.

773 Monier, E., Scott, J. R., Sokolov, A. P., Forest, C. E., and Schlosser, C. A.: An integrated
774 assessment modeling framework for uncertainty studies in global and regional climate
775 change: The MIT IGSM-CAM (version 1.0), *Geosci. Mod. Dev.*, 6, 2063–2085, 2013.

776 Monier, E., Gao, X., Scott, J. R., Sokolov, A. P., and Schlosser, C. A.: A framework for
777 modeling uncertainty in regional climate change, *Clim. Change*, 131, 51–66, 2015.

778 Monier, E., Xu, L., and Snyder, R.: Uncertainty in future agro-climate projections in the United
779 States and benefits of greenhouse gas mitigation, *Environ. Res. Lett.*, 11, 055001, 2016.

780 Paltsev, S., Reilly, J. M., Jacoby, H. D., Eckaus, R. S., McFarland, J. R., Sarofim, M. C.,
781 Asadoorian, M. O., and Babiker, M. H.: The MIT emissions prediction and policy analysis
782 (EPPA) model: Version 4, Rep. 125, MIT Joint Program on the Sci. and Policy of Global
783 Change, 2005.

784 Pogson, M., and Smith, P.: Effect of spatial data resolution on uncertainty, *Environ. Model.*
785 *Softw.*, 63, 87–96, 2015.

786 Pyle, J. A., and Zavody, A. M.: The modelling problems associated with spatial averaging, *Q. J.*
787 *R. Meteorol. Soc.*, 116, 753–766, 1990.

788 Räisänen, J., and Ylhäisi, J. S.: How much should climate model output be smoothed in space?,
789 *J. Climate*, 24, 867–880, 2011.

790 Rasmussen, D. J., Fiore, A. M., Naik, V., Horowitz, L. W., McGinnis, S. J., and Schultz, M. G.:
791 Surface ozone-temperature relationships in the eastern US: A monthly climatology for
792 evaluating chemistry-climate models, *Atmos. Environ.*, 47, 142–153, 2012.

793 Rienecker, M. M., Suarez, M. J., Gelaro, R., Todling, R., Bacmeister, J., Liu, R., Bosilovich, M.
794 G., Schubert, S. D., Takacs, L., Kim, G-K, Bloom, S., Chen, J., Collins, D., Conaty, A., da
795 Silva, A., Gu, W., Joiner, J., Koster, R. D., Lucchesi, R., Molod, A., Owens, T., Pawson, S.,
796 Pegion, P., Redder, C. R., Reichle, R., Robertson, F. R., Ruddick, A. G., Sienkiewicz, M.,
797 and Woollen, J.: MERRA: NASA’s Modern-Era Retrospective analysis for Research and
798 Applications, *J. Climate*, 24, 3624–3648, 2011.

799 Roberts, C. D., Palmer, M. D., McNeall, D., and Collins, M.: Quantifying the likelihood of a
800 continued hiatus in global warming, *Nat. Clim. Change*, 5, 337–342, 2015.

801 Schnell, J. L., and Prather, M. J.: Co-occurrence of extremes in surface ozone, particulate matter,
802 and temperature over eastern North America, *Proc. Natl. Acad. Sci. U.S.A.*, 114, 11, 2854-
803 2859, 2017.

804 Schurer, A. P., Hegerl, G. C., Mann, M. E., Tett, S. F. B., and Phipps, S. J.: Separating forced
805 from chaotic climate variability over the past millennium, *J. Climate*, 26, 6954–6973, 2013.

806 Searle, K. R., Chipperfield, M. P., Bekki, S., and Pyle, J. A.: The impact of spatial averaging on
807 calculated polar ozone loss: 2. Theoretical analysis, *J. Geophys. Res.*, 103, D19, 25409–
808 25416, 1998.

809 Sofen, E. D., Bowdalo, D., and Evans, M. J.: How to most effectively expand the global surface
810 ozone observing network, *Atmos. Chem. Phys.*, 16, 1445–1457, 2016.

811 Stevenson, D. S., Young, P. J., Naik, V., Lamarque, J. F., Shindell, D. T., Voulgarakis, A., Skeie,
812 R. B., Dalsøren, S. B., Myhre, G., Berntsen, T. K., Folberth, G. A., Rumbold, S. T., Collins,
813 W. J., MacKenzie, I. A., Doherty, R. M., Zeng, G., van Noije, T. P. C., Strunk, A.,
814 Bergmann, D., Cameron-Smith, P., Plummer, D. A., Strode, S. A., Horowitz, L., Lee, Y. H.,
815 Szopa, S., Sudo, K., Nagashima, T., Josse, B., Cionni, I., Righi, M., Eyring, V., Conley, A.,
816 Bowman, K. W., and Wild, O.: Tropospheric ozone changes, radiative forcing and
817 attribution to emissions in the Atmospheric Chemistry and Climate Model Intercomparison
818 Project (ACCMIP), *Atmos. Chem. Phys.*, 13, 3063–3085, 2013.

819 Strode, S. A., and Pawson, S.: Detection of carbon monoxide trends in the presence of
820 interannual variability, *J. Geophys. Res. Atmos.*, 118, 12257-12273, 2013.

821 Sun, J., Fu, J. S., Drake, J., Lamarque, J.-F., Tilmes, S., and Vitt, F.: Improvement of the
822 prediction of surface ozone concentration over conterminous U.S. by a computationally
823 efficient second-order Rosenbrock solver in CAM4-Chem, *J. Adv. Model Earth. Sy.*, 9,
824 482–500, 2017.

825 Tilmes, S., Lamarque, J.-F., Emmons, L. K., Conley, A., Schultz, M. G., Saunio, M., Thouret,
826 V., Thompson, A. M., Oltmans, S. J., Johnson, B., and Tarasick, D.: Technical Note:
827 Ozonesonde climatology between 1995 and 2011 : description, evaluation and applications,
828 *Atmos. Chem. Phys.*, 12, 7475-7497, 2012.

829 Tilmes, S., Lamarque, J. F., Emmons, L. K., Kinnison, D. E., Ma, P. L., Liu, X., Ghan, S.,
830 Bardeen, C., Arnold, S., Deeter, M., Vitt, F., Ryerson, T., Elkins, J. W., Moore, F.,
831 Spackman, J. R., and Val Martin, M.: Description and evaluation of tropospheric chemistry

832 and aerosols in the Community Earth System Model (CESM1.2), *Geosci. Model Dev.*, 8,
833 1395–1426, 2015.

834 Tilmes, S., Lamarque, J. F., Emmons, L. K., Kinnison, D. E., Marsh, D., Garcia, R. R., Smith, A.
835 K., Neely, R. R., Conley, A., Vitt, F., Val Martin, M., Tanimoto, h., Simpson, I., Blake, D.
836 R., and Blake, N.: Representation of the Community Earth System Model (CESM1) CAM4-
837 chem within the Chemistry-Climate Model Initiative (CCMI), *Geosci. Model Dev.*, 9,
838 1853–1890, 2016.

839 Travis, K. R., Jacob, D. J., Fisher, J. A., Kim, P. S., Marais, E. A., Zhu, L., Yu, K., Miller, C. C.,
840 Yantosca, R. M., Sulprizio, M. P., Thompson, A. M., Wennberg, P. O., Crouse, J. D., St.
841 Clair, J. M., Cohen, R. C., Laughner, J. L., Dibb, J. E., Hall, S. R., Ullmann, K., Wolfe, G.
842 M., Pollack, I. B., Peischl, J., Neuman, J. A., and Zhou, X.: Why do models overestimate
843 surface ozone in the Southeast United States?, *Atmos. Chem. Phys.*, 16, 13561–13577,
844 2016.

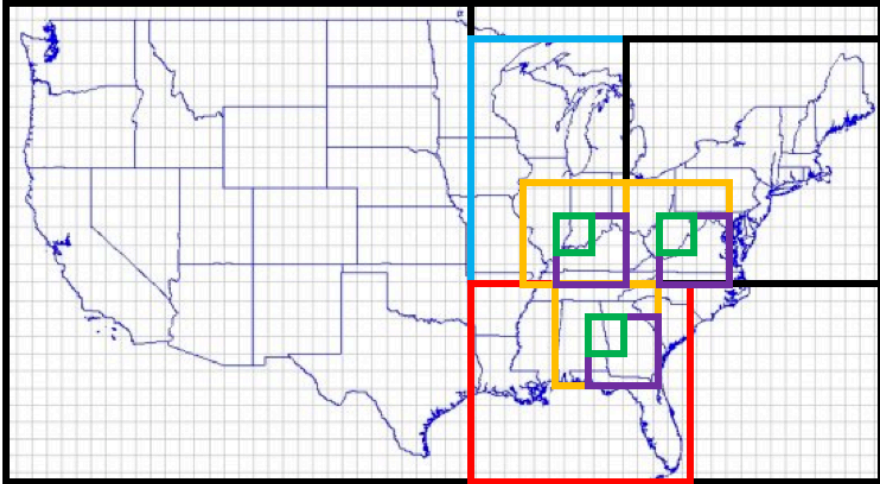
845 US EPA: National Ambient Air Quality Standards for Ozone: Final Rule. *Fed. Regist.* 80 (206),
846 65292-65468. 2015.

847 US EPA: CASTNET 2014 Annual Report Prepared by Environmental Engineering and
848 Measurement Services, Inc. for the U.S. Environmental Protection Agency, 2016.

849 Weatherhead, E. C., Stevermer, A. J., and Schwartz, B. E., Detecting environmental changes and
850 trends, *Physics and Chemistry of the Earth*, 27, 399-403, 2002.

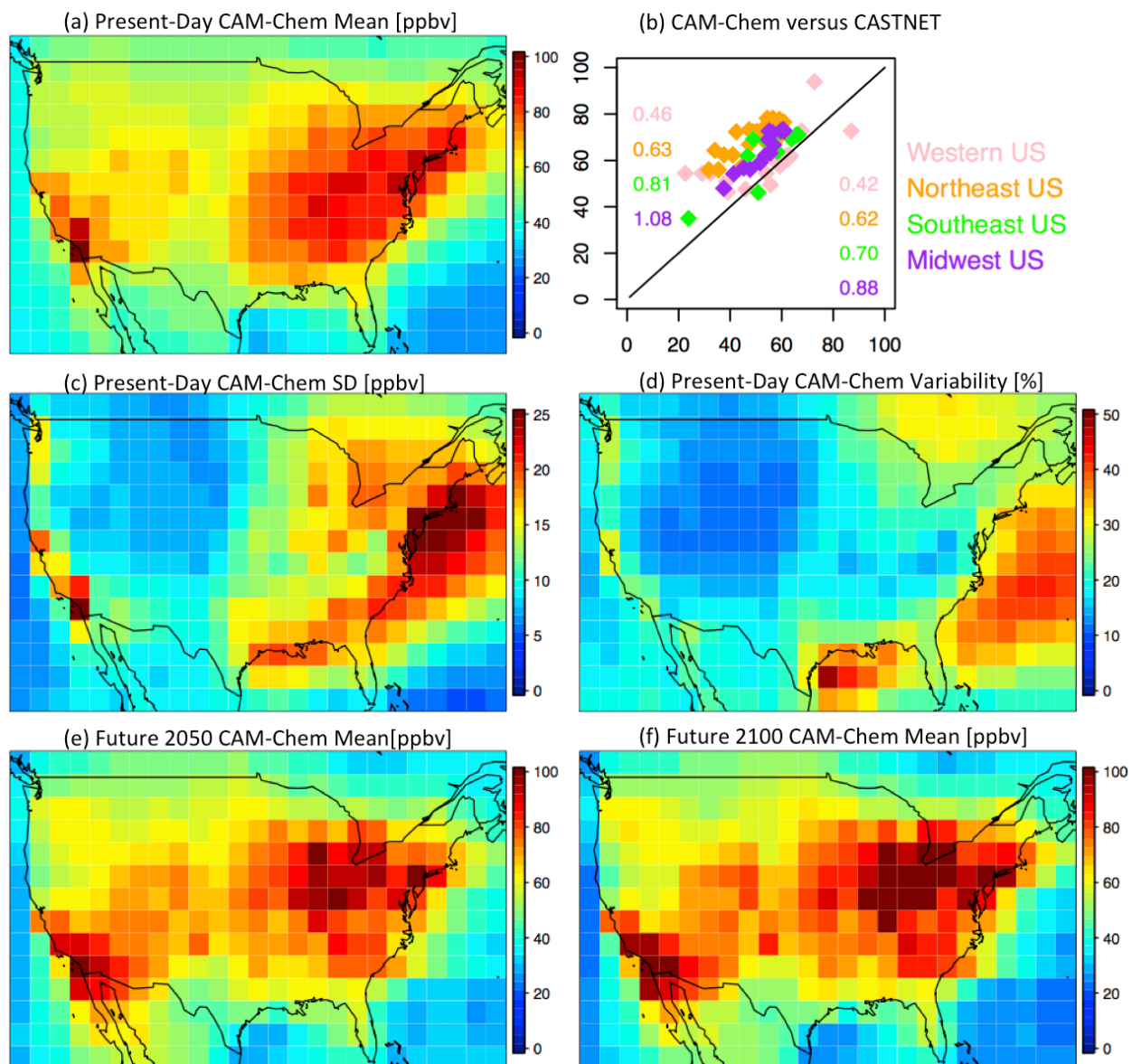
851 Wild, O., and Prather, M. J.: Global tropospheric ozone modeling: Quantifying errors due to grid
852 resolution, *J. Geophys. Res.*, 111, D11305, 2006.

853 Young, P. J., Archibald, A. T., Bowman, K. W., Lamarque, J.-F., Naik, V., Stevenson, D. S.,
854 Tilmes, S., Voulgarakis, A., Wild, O., Bergmann, D., Cameron-Smith, P., Cionni, I.,
855 Collins, W. J., Dalsøren, S. B., Doherty, R. M., Eyring, V., Faluvegi, G., Horowitz, L. W.,
856 Josse, B., Lee, Y. H., MacKenzie, I. A., Nagashima, T., Plummer, D. A., Righi, M.,
857 Rumbold, S. T., Skeie, R. B., Shindell, D. T., Strode, S. A., Sudo, K., Szopa, S., and Zeng,
858 G.: Pre-industrial to end 21st century projections of tropospheric ozone from the
859 Atmospheric Chemistry and Climate Model Intercomparison Project (ACCMIP), *Atmos.*
860 *Chem. Phys.*, 13, 2063–2090, 2013.

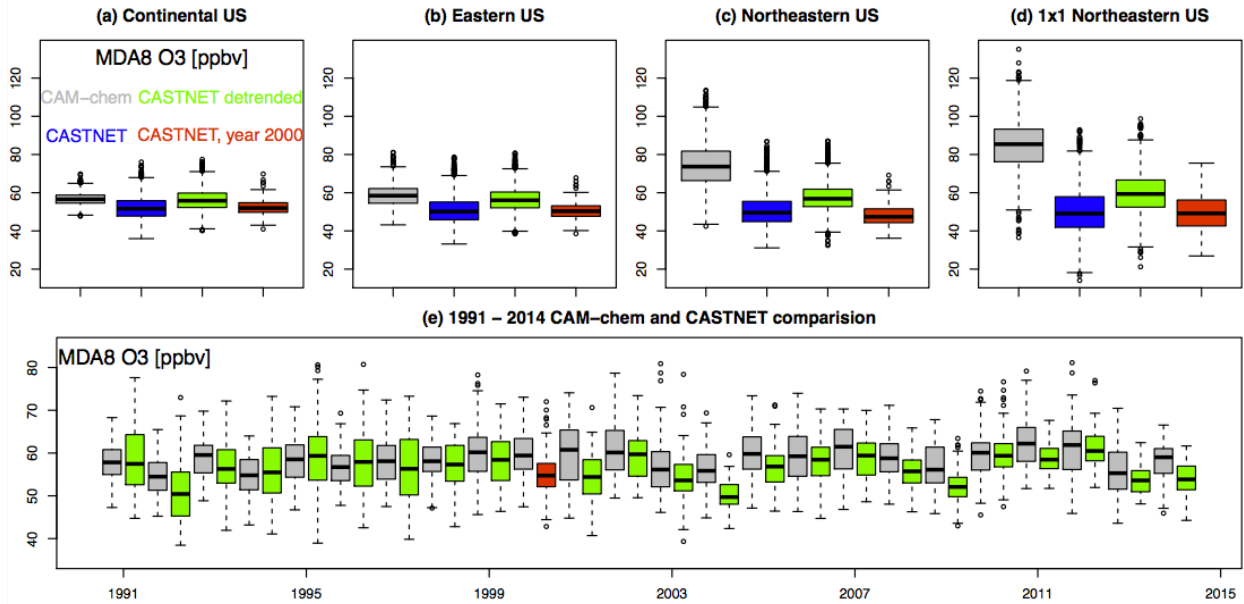


861
862
863
864
865
866
867
868

Figure 1: Telescoping Spatial Regions included in this study. The largest scale we consider is the Continental US (outer border). We focus on the Eastern US, by subdividing into three subregions: the Midwest (blue), Northeast (black), and Southeast (red). Within each subregion we telescope into a 3x3 grid cell (yellow), 2x2 grid cell (purple), and a 1x1 grid cell (green). In the paper, we only show a subset of these telescoping regions, and we include the rest in the Supplemental Material.

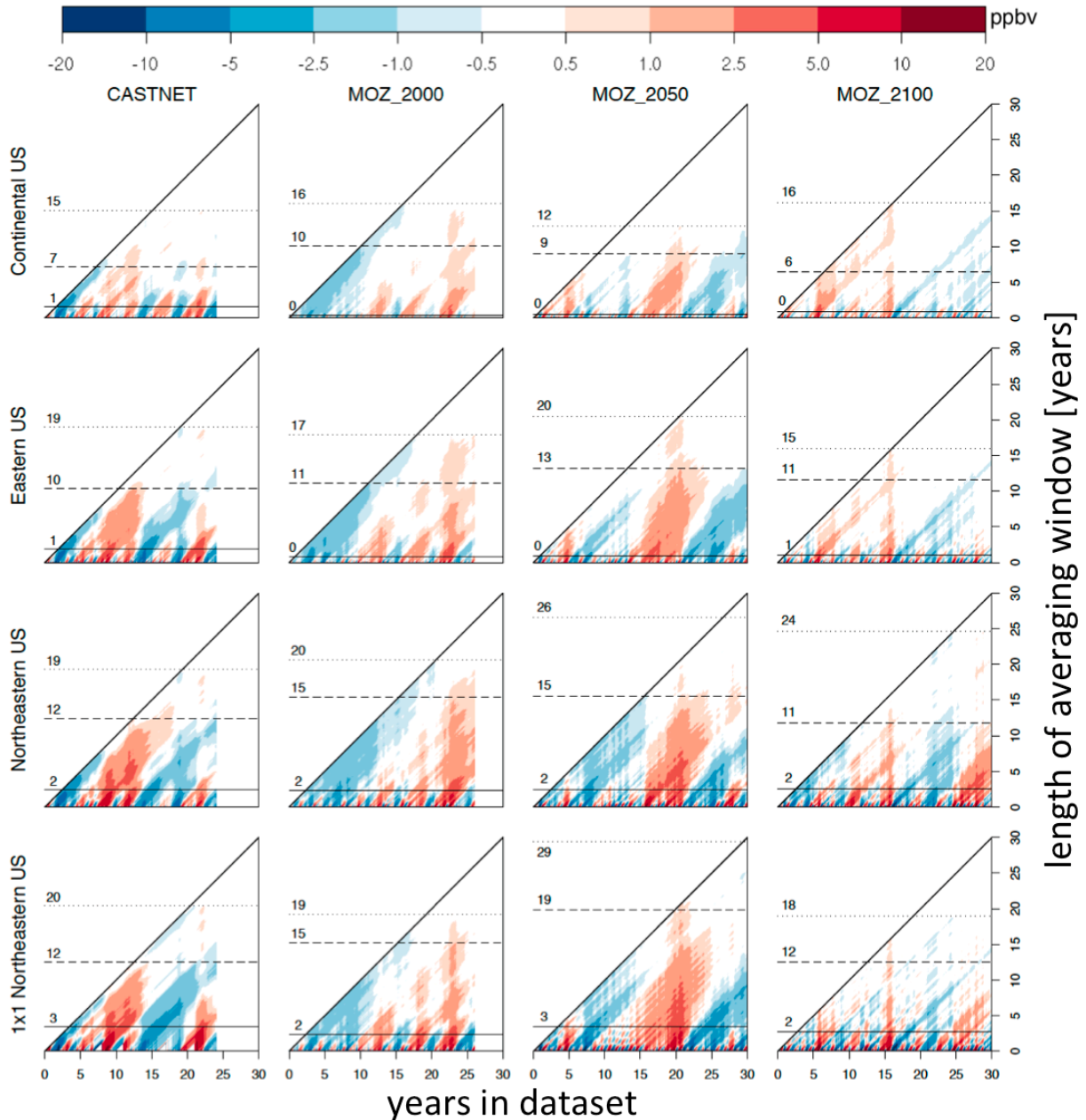


869
 870 **Figure 2: Continental US surface maps of (a) present-day CAM-chem mean MDA8 O₃; (b) CAM-Chem (y-**
 871 **axis) comparison to CASTNET observations (x-axis) for the year 2000 (see Brown-Steiner et al. (in review)**
 872 **for additional comparisons); (c) present-day CAM- chem standard deviation of MDA8 O₃; (d) present-day**
 873 **CAM- chem variability (standard deviation divided by mean, as a percent); (e) future CAM- chem year 2050**
 874 **mean MDA8 O₃; and (f) future CAM- chem year-2100 mean MDA8 O₃. All model results are averaged over**
 875 **every JJA day in the time series, while the CASTNET results are only for the year 2000. The numbers in**
 876 **Figure 2b are slopes (left) and R² values (right).**
 877



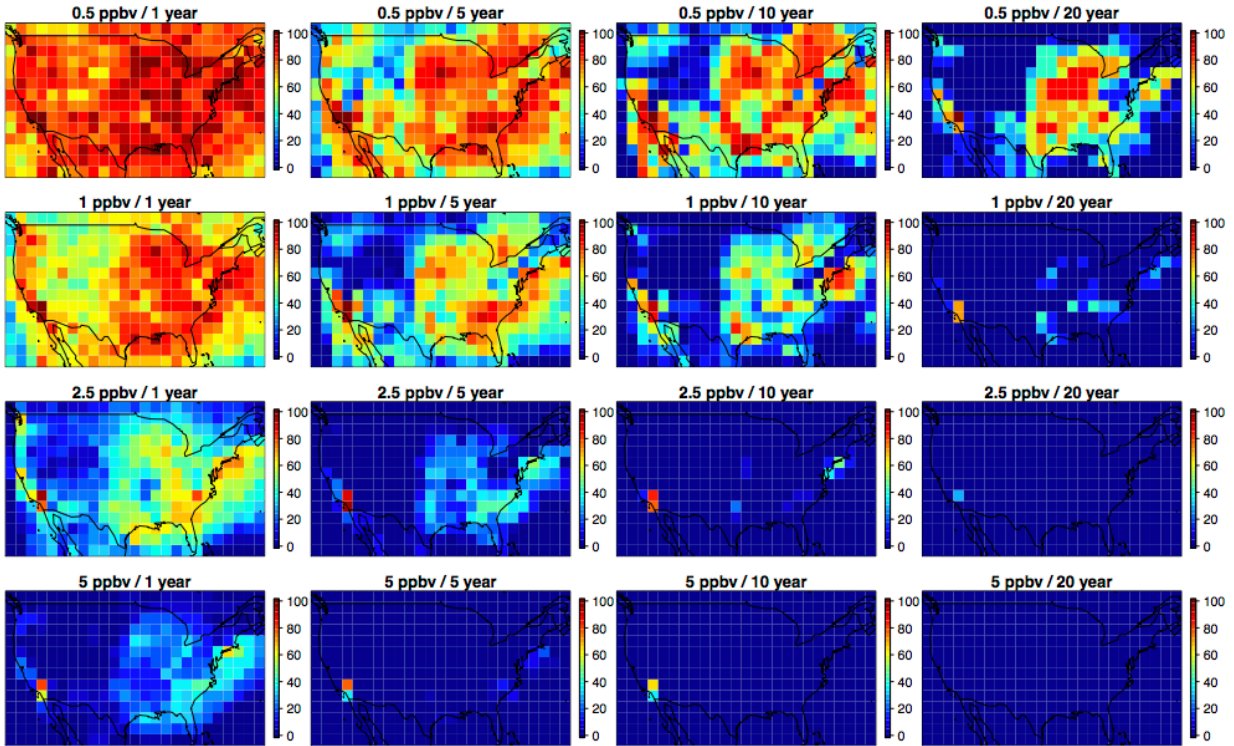
878
 879
 880
 881
 882
 883
 884
 885
 886
 887
 888
 889
 890
 891

Figure 3: (a-d): Boxplots for surface MDA8 O₃ for every summertime (JJA) day from 1991 – 2014 averaged over the Continental US, the Eastern US, the Northeastern US, and a single grid cell in the Northeastern US from CAM-chem (grey), CASTNET observations (blue), detrended CASTNET observations centered at the year 2000 (green), and since the CAM-chem simulations have cycled year-2000 emissions and boundary conditions, the CASTNET values for the year 2000 only (red). (e) Comparison of the yearly JJA MDA8 O₃ estimates averaged over the Eastern US for CAM-chem (grey) and the detrended CASTNET (green) from 1991 – 2014. The single red boxplot coincides with the red boxplot in (b). The units are in ppbv, and for each boxplot the box contains the Inter Quartile Range (IQR), the horizontal line within the box is the median, and the whiskers extend out to the farthest point which is within 1.5 times the IQR with circles indicating any outliers.



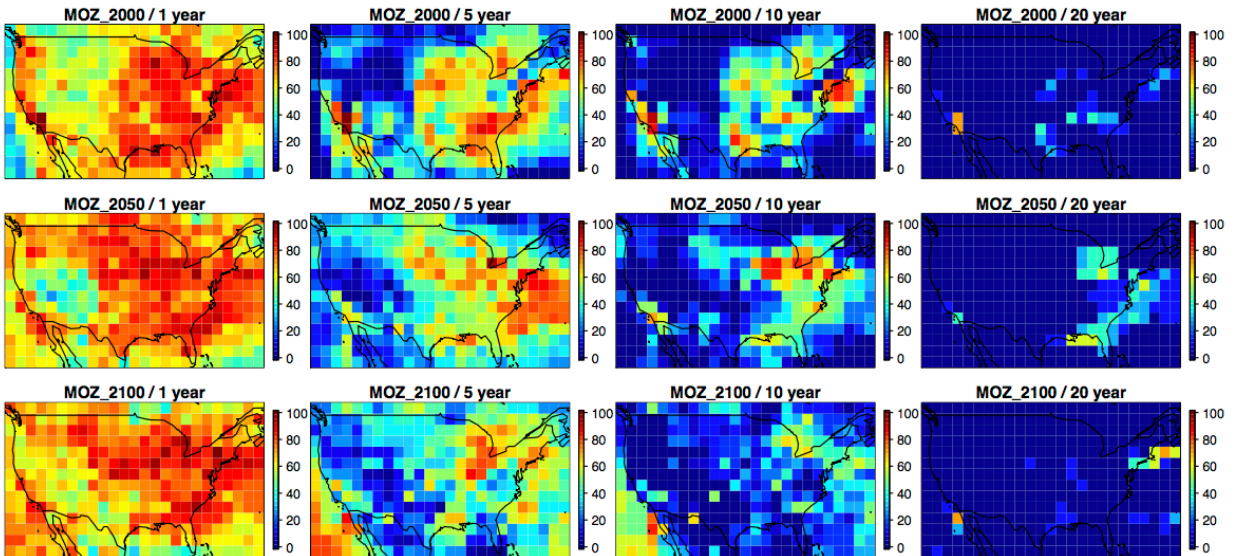
892
893
894
895
896
897
898
899
900
901
902
903
904
905

Figure 4: Comparisons of the variability represented by the summertime MDA8 O₃ anomaly (from the long-term summertime mean) for the four datasets in this study (CASTNET, MOZ_2000, MOZ_2050, MOZ_2100, columns) averaged over the four telescoping regions (CUS, EUS, NEUS, NEUS 1x1, rows). In each panel, the horizontal axis is the number of years in the dataset (24 years (1991-2014) for CASTNET, 26 years (1990-2015) for MOZ_2000, and 30 years (2036-2065 and 2086-2115) for MOZ_2050 and MOZ_2100), and the vertical axis represents the length of the averaging window (ranging from 1 day (bottom row) up to the entire time series (top pixel)). Each pixel represents the estimate of the ozone anomaly for a given averaging window (vertical axis) ending at a given time (horizontal axis). Horizontal lines indicate the length of averaging window required to guarantee that the variability drops below thresholds of 5 ppbv (solid), 1 ppbv (dashed), and 0.5 ppbv (dotted).



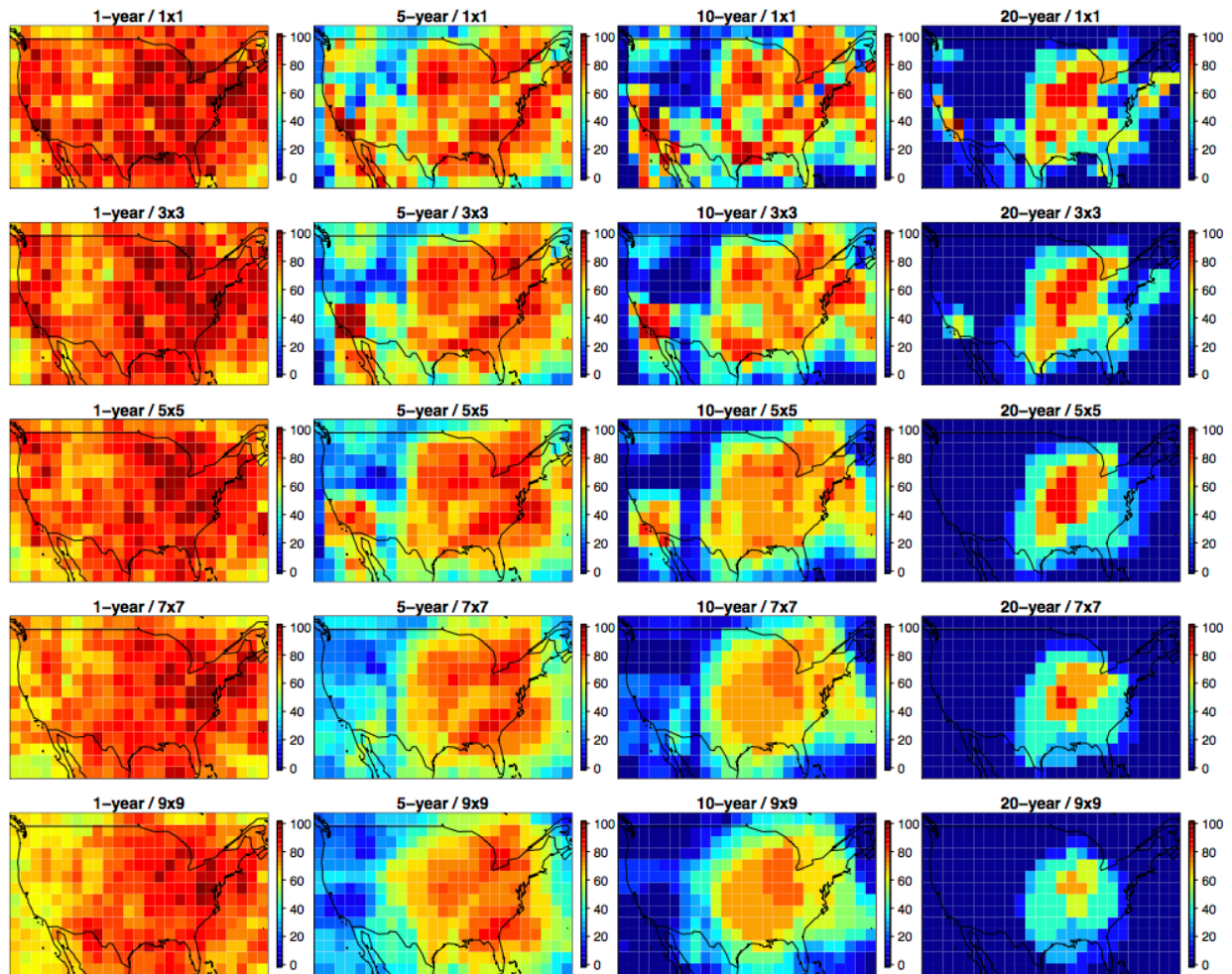
906
907
908
909
910
911
912

Figure 5: Spatial Plots over the Continental US plotting the likelihood (%) that an estimate of ozone exceeds a given threshold due to meteorological variability (rows) at the grid-cell level when using different lengths of averaging windows (columns) for the present-day CESM simulation (MOZ_2000).

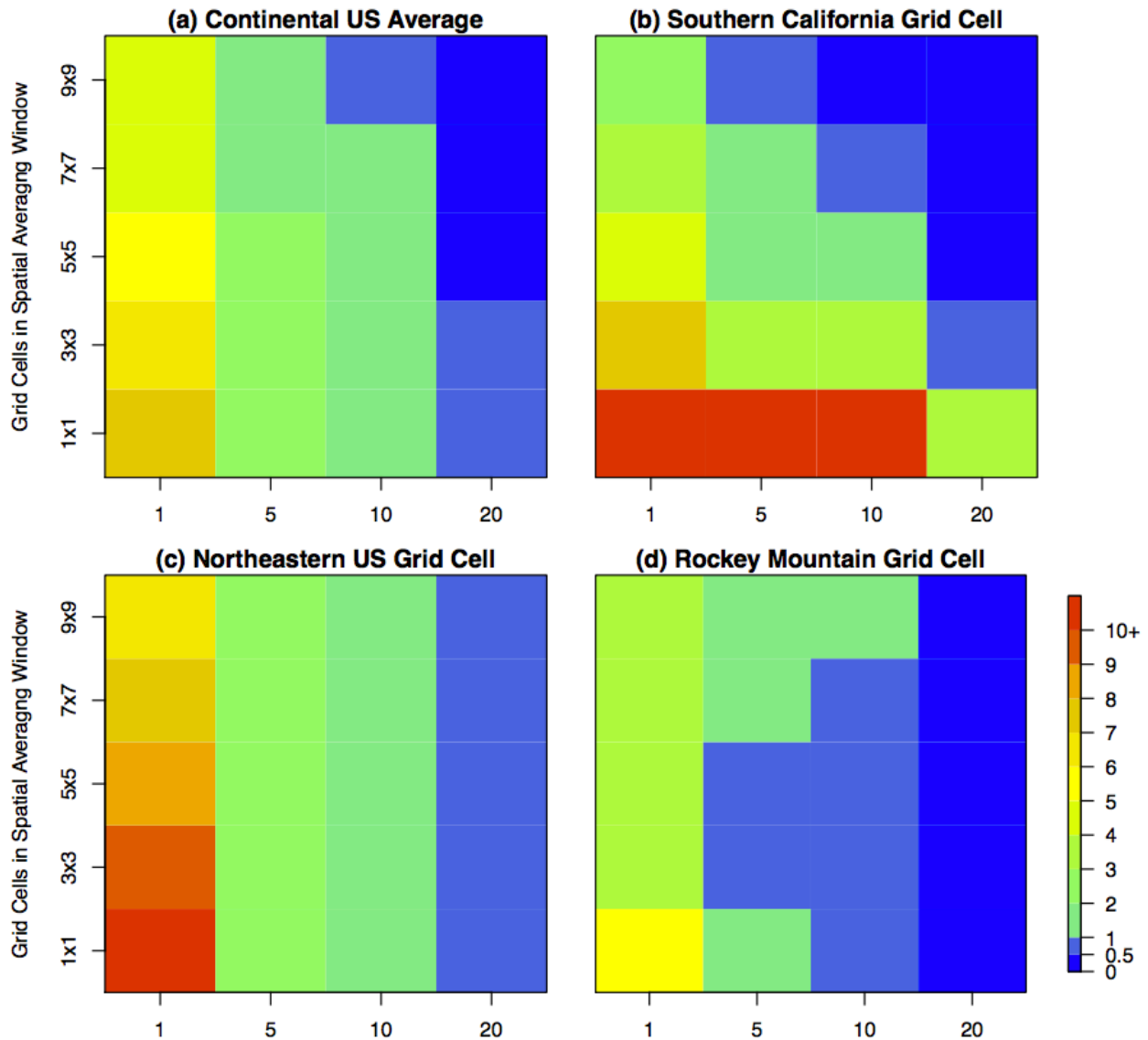


913
914
915
916
917

Figure 6: As in Figure 5, but only the second row (1 ppbv threshold), for present-day CAM-chem (MOZ_2000), future CAM-chem 2050 (MOZ_2050), and future CAM-chem 2100 (MOZ_2100).



918
 919 **Figure 7: Combined impact of temporal and spatial averaging on reducing ozone variability on the**
 920 **likelihood (%) of exceeding the 0.5 ppbv threshold (as in Figures 5, 6, and Supplemental Figure S3)**
 921 **for the present-day MOZ_2000 simulation. The top row is the same as in Figure 6, while the lower rows**
 922 **have averaged the values within a 3x3, 5x5, 7x7, and 9x9 grid box surrounding each individual grid cell.**
 923



925

926 **Figure 8:** The maximum potential calculated MDA8 O₃ anomaly [ppbv] from the long-term mean for (a)
 927 the Continental US average and three individual grid cells taken from (b) Southern California,
 928 demonstrating effective temporal and spatial averaging, (c) the Northeast, where spatial averaging is
 929 ineffective, and (d) the Rocky Mountains, where spatial averaging initially reduces the anomaly, but
 930 then increases the anomaly as surrounding regions get included in the spatial average. The number of
 931 years included in the temporal averaging window increase along the x-axis and the number of grid cells
 932 included in the spatial averaging window increase along the y-axis. A full map of the Continental US can
 933 be found in the Supplemental Material (Figure S4). Note that the color scale is non-linear, and the color
 934 transitions are selected to match the thresholds established throughout this paper.
 935

			CASTNET	MOZ_2000	MOZ_2050	MOZ_2100
Continental US	Mean	ppbv	52.4	56.7	56.8	57.4
	Standard Deviation	ppbv	5.04	3.08	3.54	3.73
	Variability	%	10%	5%	6%	7%
	Bias	ppbv		4.31		
Eastern US	Mean	ppbv	50.7	58.6	55.5	56.5
	Standard Deviation	ppbv	5.78	5.77	5.80	6.50
	Variability	%	11%	10%	10%	12%
	Bias	ppbv		7.91		
Northeastern US	Mean	ppbv	48.3	74.4	68.4	73.0
	Standard Deviation	ppbv	6.89	11.4	11.1	12.7
	Variability	%	14%	15%	16%	17%
	Bias	ppbv		26.1		
1x1 Northeastern US	Mean	ppbv	49.6	84.9	81.1	85.1
	Standard Deviation	ppbv	10.2	12.8	16.7	17.3
	Variability	%	21%	15%	21%	20%
	Bias	ppbv		35.3		

Table 1: Statistical Summary of the CASTNET observations and the three CAM-chem simulations for different spatial averaging regions within the US. Variability is defined as the standard deviation divided by the mean value (in percent). Biases are only included for the present-day CAM-chem simulation compared to the CASTNET data. Similar tables for the other regions in this study are included in the Supplemental Material.

936
937
938
939
940
941
942
943